







Cite this: *Nanoscale*, 2019, **11**, 2056

# Influence of surface chemistry on optical, chemical and electronic properties of blue luminescent carbon dots†

Jian Ren, <sup>a,b</sup> Fabian Weber, <sup>a,c</sup> Florian Weigert,<sup>d</sup> Yajie Wang,<sup>e</sup>  
Sneha Choudhury,<sup>a,c</sup> Jie Xiao,<sup>a</sup> Iver Lauermaann, <sup>e</sup> Ute Resch-Genger, <sup>d</sup>  
Annika Bande <sup>a</sup> and Tristan Petit <sup>\*a</sup>

Carbon dots have attracted much attention due to their unique optical, chemical and electronic properties enabling a wide range of applications. The properties of carbon dots can be effectively adjusted through modifying their chemical composition. However, a major challenge remains in understanding the core and surface contributions to optical and electronic transitions. Here, three blue luminescent carbon dots with carboxyl, amino and hydroxyl groups were comprehensively characterized by UV-vis absorption and emission spectroscopy, synchrotron-based X-ray spectroscopy, and infrared spectroscopy. The influence of the surface functionality on their fluorescence was probed by pH-dependent photoluminescence measurements. Moreover, the hydrogen bonding interactions between water and the surface groups of carbon dots were characterized by infrared spectroscopy. Our results show that both core and surface electronic states of blue luminescent carbon dots contribute to electronic acceptor levels while the chemical nature of the surface groups determines the hydrogen bonding behavior of the carbon dots. This comprehensive spectroscopic study demonstrates that the surface chemistry has a profound influence on the electronic configuration and surface–water interaction of carbon dots, thus affecting their photoluminescence properties.

Received 24th October 2018,  
Accepted 21st December 2018

DOI: 10.1039/c8nr08595a

rsc.li/nanoscale

## Introduction

Carbon dots (CDs) commonly consist of a carbogenic core stabilized with ligands and/or surface groups.<sup>1,2</sup> The graphitic, amorphous or polymeric core determines the type of CD, and

the surface chemistry controls the colloidal stability and enables subsequent functionalization required for many applications.<sup>3,4</sup> Due to their unique and tunable physicochemical properties, particularly the outstanding optical properties, and excellent biocompatibility, CDs have been demonstrated to be suitable for a wide range of applications in biological imaging,<sup>5–7</sup> light emitting<sup>8–10</sup> and energy harvesting<sup>11–13</sup> among others.

Surface functionalization of CDs is of vital importance for many applications. Depending on the surface moieties, the surface-related electronic acceptor levels,<sup>14–16</sup> hydrogen bond (HB) interactions with solvent molecules can be modulated,<sup>17–19</sup> affecting the photoluminescence (PL) properties of CDs. Extensive studies of surface-related optical transitions based on UV-vis absorption and emission spectroscopy have been conducted to elucidate fluorescence mechanisms. PL with pH dependence can be monitored to assess the effect of surface groups on optical properties, which is a widely reported phenomenon for CDs.<sup>20–22</sup> On the other hand, no direct measurement of electronic transitions on surface-modified CDs has been conducted so far to our knowledge. No spectroscopic evidence of hydrogen bonding between CDs and solvent molecules beyond indirect PL measurements is available either.

<sup>a</sup>Institut Methoden der Materialentwicklung, Helmholtz-Zentrum Berlin für Materialien und Energie GmbH (HZB), Albert-Einstein-Straße 15, 12489 Berlin, Germany. E-mail: tristan.petit@helmholtz-berlin.de

<sup>b</sup>Department of Physics, Freie Universität Berlin, Arnimallee 14, 14195 Berlin, Germany

<sup>c</sup>Institute of Chemistry and Biochemistry, Freie Universität Berlin, Takustraße 3, 14195 Berlin, Germany

<sup>d</sup>Division 1.2 Biophotonics, Federal Institute for Materials Research and Testing (BAM), Richard-Willstätter Straße 11, 12489 Berlin, Germany

<sup>e</sup>Kompetenzzentrum Dünnschicht- und Nanotechnologie für Photovoltaik Berlin, Helmholtz-Zentrum Berlin für Materialien und Energie GmbH (HZB), Schwarzschildstraße 3, 12489 Berlin, Germany

†Electronic supplementary information (ESI) available: UV-vis absorption spectra, and non-normalized PL spectra of CDs, interpretation of C K edge XA spectra of carbon dots based on local time-dependent DFT calculations, C K-edge K $\alpha$  XE spectra, O K-edge XA/XE spectra of the three CD samples, N K-edge XA/XE spectra of CDs-NH<sub>2</sub>, XPS results, second derivative of IR spectra of the three CD samples, and technical details of three CD samples. See DOI: 10.1039/c8nr08595a



Extending the characterization of CDs with complementary spectroscopy techniques is strongly needed for a deeper understanding of the structure–property relationship of CDs. In particular, synchrotron-based soft X-ray spectroscopies are a powerful technique for exploring element-specific electronic states and chemical structures of carbon nanomaterials. Soft X-ray absorption spectroscopy (XAS) and X-ray emission spectroscopy (XES) can provide detailed information about the partially unoccupied and occupied electronic states, respectively.<sup>23</sup> In combination with X-ray photoelectron spectroscopy (XPS), which has been frequently used to probe the core levels of carbon, oxygen and nitrogen in CDs,<sup>21,24,25</sup> these methods can provide a complete picture of electronic states in CDs. No reports of XAS/XES on carbon dots are though available at the moment to our knowledge.

In addition, Fourier transform infrared (FTIR) spectroscopy is highly sensitive to chemical bonding and surface functional groups and has been extensively applied to characterize the chemical structure of CDs. Nevertheless, FTIR using an attenuated total reflectance (ATR) environmental cell can also enable the direct detection of chemical changes under various conditions.<sup>26</sup> We previously demonstrated that monitoring the OH vibrations of water molecules during exposure to humid air using ATR-FTIR was a sensitive method for probing the HB environment around carbon nanomaterials.<sup>27</sup> Only surface groups are expected to interact with water molecules; therefore exposure to humid air could also be used to identify surface-related chemical groups and the HB acceptor/donor nature.

In this work, the optical properties of three commercial blue luminescent CDs functionalized with carboxyl (CDs-COOH), amino (CDs-NH<sub>2</sub>) and hydroxyl (CDs-OH) groups are determined by UV-vis absorption and PL measurements and compared. Subsequently, their electronic structures are characterized by XAS and XES. The interpretation of XA spectra is discussed based on density functional theory calculations. Moreover, XPS was applied to align the XA and XE spectra at C, N and O K-edges to the Fermi level to estimate the contribution of each atom to the valence and conduction bands. In addition, the chemical structures of the CDs and HB interactions with water molecules were characterized by ATR-FTIR spectroscopy. Finally, we attempt to correlate these results with the PL properties of differently functionalized CDs.

## Results and discussion

### Optical properties of carbon dot samples

The broad absorption spectra and the much more structured emission spectra of the three CDs are shown in Fig. 1. The closely resembling absorption spectra of the three CD samples reveal a well-resolved peak at around 340 nm (Fig. 1), which originates from the C=O bonds of the carbonyl and/or carboxyl groups in the carbogenic core or from COOH groups. The higher energy absorption feature in the region 220–250 nm (Fig. S1, ESI†) is associated with the optical tran-

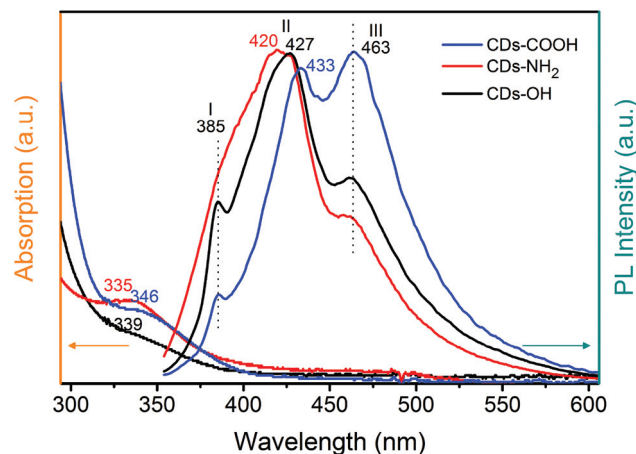


Fig. 1 UV-Vis absorption and emission spectra of blue luminescent carbon dots. Excitation was at 338 nm.

sition in the carbon core.<sup>9</sup> The fluorescence intensities follow the order CDs-NH<sub>2</sub> > CDs-OH > CDs-COOH from the strongest to the weakest (Fig. S2, ESI†). The PL spectra in Fig. 1 obtained upon UV excitation exhibit three distinct emission peaks at around 385 (I), 420–433 (II), and 463 nm (III). According to previous studies, these emissions I, II and III can be attributed to  $n-\sigma^*$  (such as C–O–C, C–OH or C–N),  $n-\pi^*$  (in C=O), and  $\pi-\pi^*$  transitions in the graphitic core, respectively.<sup>15,22</sup> A more profound assignment of the origin of the optical properties of CDs is hampered by the different synthetic routes used to prepare the commercial CDs, which also complicates the evaluation of the exact role played by the different surface groups. These challenges are addressed in the following by the detailed characterization of the samples using different analytical techniques, particularly X-ray spectroscopy.

### Electronic structure of carbon dot samples

X-ray spectroscopy was employed to determine the local electronic configurations and chemical structures of different blue luminescent CDs. Note that X-ray spectroscopy is sensitive to both core and surface contributions of the CDs due to their small size. The XA spectra of the three CD samples at the C K-edge are compared in Fig. 2. Four main features at 285.2 (A), 287.5 (B), 288.9 (C) and 294–297 (D) eV are observed. In addition, DFT calculations using an individual-atom decomposition method were performed,<sup>28</sup> to enable the assignment of the different features of the C K-edge XA spectra (see Table S1, ESI†). According to the calculation and previous experimental studies on carbon nanomaterials, feature A at 285.2 eV can be assigned univocally to the excitation of core electrons into  $\pi^*_{C=C}$  orbitals.<sup>29</sup> Depending on the chemical environment of the core orbitals, *i.e.* the functionalization of the carbon atom, one finds shifts with respect to the exact position of the expected signal (Table S1, ESI†). Feature B is typical of the transition to the  $\pi^*$  orbital of C–O–C in an epoxide structure<sup>29,30</sup> but a contribution from  $\pi^*$  of C–COH bonds in the hydroxyl



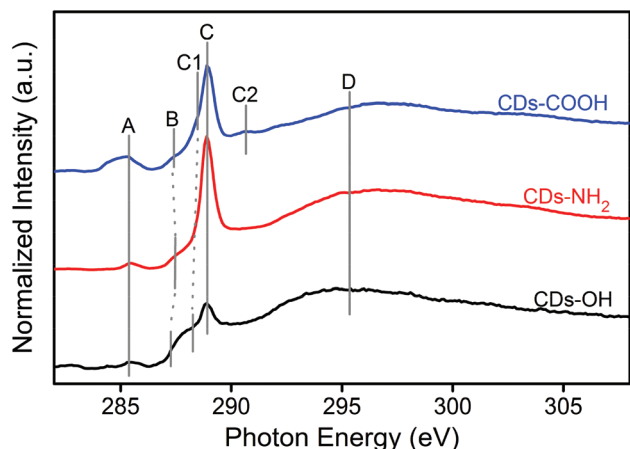


Fig. 2 XA spectra at the C K-edge of carbon dots with different surface chemistries.

group is also possible.<sup>31,32</sup> The sharp peak at 288.9 eV (C) is mainly attributed to both  $\pi^*_{\text{C=O}}$  excitation processes in carboxyl and/or carbonyl groups and  $\sigma^*_{\text{O-H}}$  transitions in the OH group.<sup>32,33</sup> Signal C1 at 288.4 eV can be attributed to additional  $\pi^*_{\text{C=C}}$  transitions in  $\text{sp}^2$  bridge and edge positioned carbon atoms<sup>34</sup> as well as  $\pi^*_{\text{C=O}}$  transitions.<sup>29</sup> At 290.6 eV, one can find the feature C2 in the CDs-COOH sample, which is best assigned to  $\sigma^*_{\text{C-O}}$  transitions in carboxylated carbon atoms, based on the theoretical calculations. In different publications<sup>30,31,34</sup> this signal is described as  $\pi^*_{\text{O-C=O}}$  transition, which can be supported by calculations. It shall be mentioned that both features C and C2 lie also in the typical range for various  $\sigma^*_{\text{C-H}}$  transitions, which leads to the increase in the background intensity. Finally, feature D in the range of 294–297 eV is related to all kinds of  $\sigma^*_{\text{C-C}}$  and  $\sigma^*_{\text{C-O}}$  transitions.

XES is complementary to XAS as the observed spectral shape reflects the partial density of occupied states. Fig. S2 (ESI†) presents the non-resonant C K $\alpha$  XE spectra of CD samples. The general profiles in the C K $\alpha$  XE spectra are similar for CDs-COOH and CDs-NH<sub>2</sub>. All spectra exhibit a broad feature, which is associated with the  $\sigma$  state and centered at approximately 277.2 eV, and a high-energy shoulder, which is associated with the  $\pi$  state and centered close to 280.8 eV. For CDs-OH, the  $\sigma$  and  $\pi$  features locate respectively around 278.4 eV and 280.3 eV.<sup>29,32</sup>

The O K-edge XA/XE spectra of the three CD samples (Fig. 3 and S3†) and N K-edge XA/XE spectra of CDs-NH<sub>2</sub> (Fig. 3 and S4†) provide supplementary information regarding the chemical bonding of oxygen and nitrogen atoms. In the O K-edge XA spectra, the sharp peaks at 533.8 eV (CDs-NH<sub>2</sub> and CDs-OH) or 534 eV (CDs-COOH), together with the feature shown at the left shoulder (532.9 eV), are  $\pi^*$  resonances from C=O bonds.<sup>35,36</sup> Besides, a shoulder at 535.1 eV for O 1s  $\rightarrow \pi^*_{\text{C-OH}}$  of the carboxyl groups is clearly observed for CDs-COOH. The feature at 537 eV can be ascribed to transitions from O 1s core levels to  $\pi^*$  states in epoxy configurations. The  $\sigma^*$  feature,

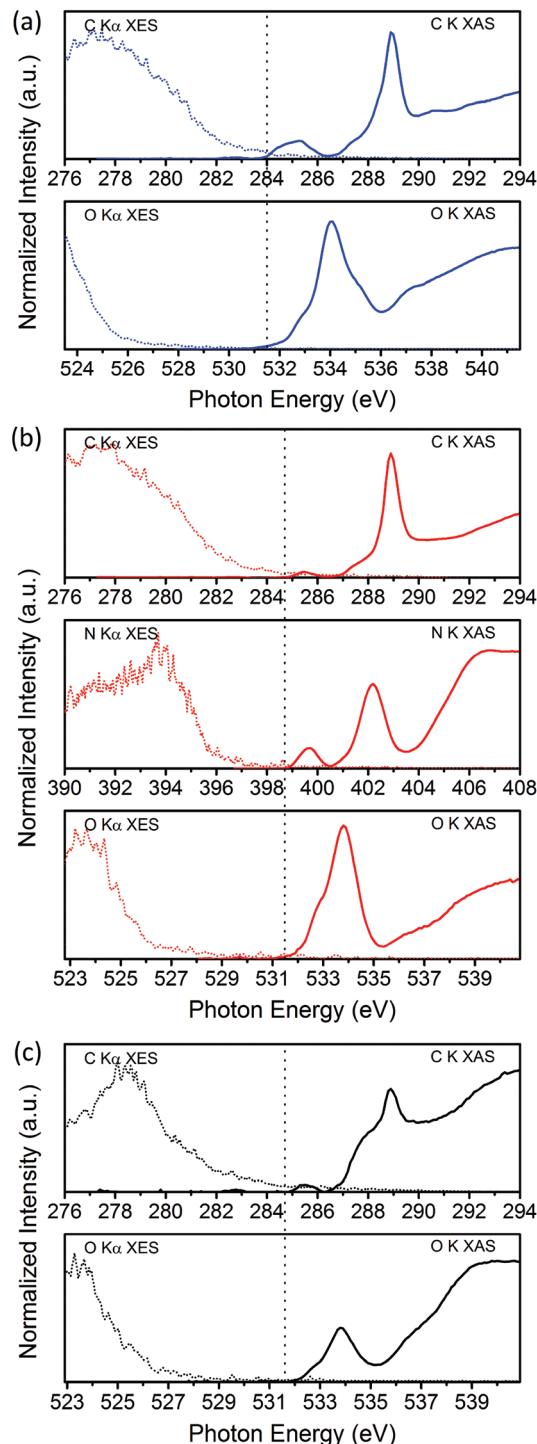


Fig. 3 C, N and O K-edge XA/XE spectra in the vicinity of the band gaps of (a) GQDs-COOH, (b) GQDs-NH<sub>2</sub>, and (c) GQDs-OH. The dotted line shows the estimated Fermi level based on XPS measurements.

which appears at a higher energy region (539–550 eV) consists of C–O, O–H, C=O and epoxide groups.<sup>37,38</sup> The distinguishable feature at 545.3 eV for 1s  $\rightarrow \sigma^*_{\text{C=O}}$  in carboxyl groups is only observed in CDs-COOH (Fig. S3, ESI†).<sup>35</sup> In the N K-edge XA spectrum of CDs-NH<sub>2</sub>, the contribution of nitrogen to the



electronic configuration and local structure in CDs-NH<sub>2</sub> is evidenced by two sharp features at 399.7 eV and 402.2 eV, which arise from transitions of N 1s to unoccupied  $\pi^*$  states of pyridinic (or pyrrolic) nitrogen and quaternary nitrogen. The broad feature above 406 eV is attributed to the transitions to  $\sigma^*$  states of different nitrogen bonds.<sup>38,39</sup>

XPS measurements of the C 1s, N 1s and O 1s core levels of the three differently functionalized CDs (Fig. S5, ESI†) confirm the differences in the chemical and electronic states. All three CD materials have a high oxygen content (see Table S2, ESI†), which is most likely widely distributed between the carbogenic core (carbonyl and epoxide groups) and the surface (hydroxyl and carboxyl groups).<sup>2,40</sup> Using XPS results, C, N and O XA/XE spectra could be aligned to a common energy axis by offsetting XA/XE spectra using their corresponding XPS core-hole binding energies referenced to the Fermi level (Fig. 3).<sup>41–43</sup> The Fermi level is estimated for each edge by measuring the lowest binding energy peak of the respective core levels (Fig. S5, ESI†). In the vicinity of the band gap, electronic states contributing to valence and conduction bands can be identified. For all CDs, the C K-edge XES onset occurs at higher energy than that of the O K-edge, which means that the carbon atoms contribute more to the density of states (DOS) in the valence band. For CDs-NH<sub>2</sub>, the N K-edge XES onset is sharper with a greater spectral weight at 4 eV below the Fermi level; therefore N atoms may also contribute significantly to occupied states. Previous studies have confirmed that introducing nitrogen atoms, as an electron-donating element, into CDs,<sup>44</sup> graphene<sup>45</sup> and other carbon nanomaterials<sup>32</sup> could modulate the valence band edge or create midgap states, leading to a narrower band gap.

For the conduction band region, the  $\pi^*$  transition from  $sp^2$  carbon in the C K-edge XAS is located at lower energy than the first unoccupied states of the O K-edge XAS, indicating that carbon atoms in the graphitic core dominate the DOS in conduction bands, in particular for CDs-COOH, for which the  $\pi^*$  feature is more visible. The unoccupied states from nitrogen atoms are located closer to the edge than those from carbon and oxygen atoms in CDs-NH<sub>2</sub>. For CDs-OH, both carbon and oxygen atoms may contribute to the conduction band minimum since the first unoccupied states have similar relative energy with respect to the Fermi level.

### Chemical composition of carbon dot samples

The previous discussion about the electronic structures of the three CDs can be completed by ATR-FTIR spectroscopy. As shown in Fig. 4, the ATR-FTIR spectra of the CDs with different surface termination, characterized under dry air flow, have different vibrational signatures, coming presumably from both surface groups and carbogenic core. Peaks at 1122 cm<sup>-1</sup> and 1174 cm<sup>-1</sup> in the CDs-COOH sample and at 1260 cm<sup>-1</sup> in CDs-OH are recognized as C–O stretching vibrations in different bonding environments.<sup>25</sup> The peak at 1226 cm<sup>-1</sup> in CDs-NH<sub>2</sub> is most likely related to C–N stretching.<sup>46</sup> The features around 1390 cm<sup>-1</sup> are attributed to the bending modes of O–H and/or C–H in CDs-COOH and CDs-OH.<sup>47</sup> The feature

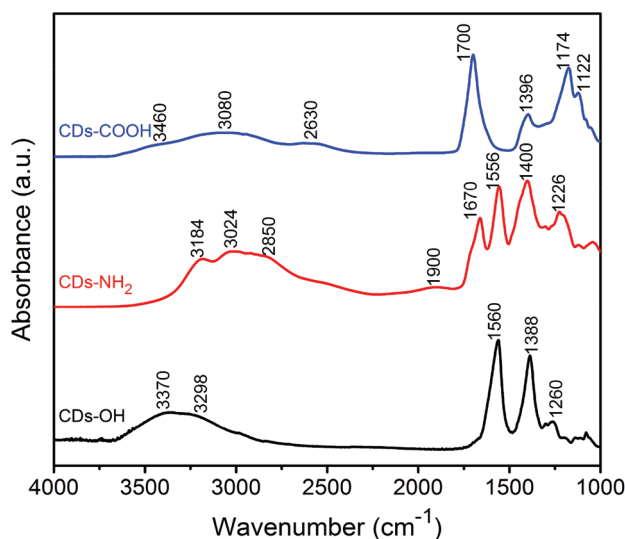


Fig. 4 ATR-FTIR spectra of CDs with different surface chemistries measured under dry air flow.

at 1400–1450 cm<sup>-1</sup> in CDs-NH<sub>2</sub> is assigned to CH<sub>2</sub> bending.<sup>13,48</sup>

All CDs contain a significant amount of C=O bonds based on X-ray spectroscopy results; however FTIR shows that they are in different chemical environments. A strong band for C=O vibrations is observed at 1556 and 1560 cm<sup>-1</sup> in CDs-NH<sub>2</sub> and CDs-OH, respectively, associated with carbonyl groups in their carbogenic core.<sup>49</sup> In this region, the IR spectrum of CDs-NH<sub>2</sub> shows two clear features at 1556 and 1670 cm<sup>-1</sup>, where the former arises primarily from the C=O stretching vibrations in the carbon core and the latter is attributed to the bending vibration mode of the NH<sub>2</sub> group.<sup>48</sup> A sharp feature at 1700 cm<sup>-1</sup> for CDs-COOH was associated with C=O stretching vibrations from surface carboxyl groups.<sup>13</sup> For CDs-NH<sub>2</sub>, the overtone bands of the amino group at 1900 cm<sup>-1</sup> can be detected.

Broad bands observed in the region of 2800–3000 cm<sup>-1</sup> for all CD samples are most likely associated with C–H stretching vibrations. In the higher frequency region around 3000–3600 cm<sup>-1</sup>, stretching modes of hydroxyl or amino groups and residual adsorbed water are expected. It should be noted that, unlike the band observed for the hydroxyl group of CDs-OH, the O–H stretching in the carboxyl groups of CDs-COOH appears as a very broad absorbance in the region 2400–3200 cm<sup>-1</sup>, which is attributed to the formation of intramolecular HBs among carboxylic groups.<sup>47</sup> The band at 3460 cm<sup>-1</sup> could result from O–H stretching of strongly adsorbed water on CDs-COOH. Adsorbed residual water was also observed from the O 1s XPS result (Fig. S5a, ESI†). In addition, the low C=O stretching frequency (1700 cm<sup>-1</sup>) of COOH groups also corroborates the strong water adsorption on CDs-COOH since the C=O stretching frequency is known to decrease by hydrogen bonding with carboxyl groups.<sup>50</sup> The asymmetrical broadening of the C=O band peak toward lower





frequency is due to the O–H bending mode of these strongly adsorbed water molecules, which is observed at  $1650\text{ cm}^{-1}$  on the second derivative of the IR spectrum (Fig. S6, ESI†). These results clearly indicate that water could be adsorbed on the CDs-COOH surface even under dry air flow at room temperature.

### Surface-dependent hydrogen bonding interactions with water

In order to estimate the ability of surface groups to form HBs with water molecules, the CDs were characterized *in situ* by recording FTIR spectra during exposure to humid air. Fig. 5a–c present the ATR-FTIR spectra of CDs-COOH, CDs-NH<sub>2</sub> and CDs-OH plotted with respect to the increase in the relative humidity (RH). To compensate the overall signal decrease, the IR spectra recorded under dry air (RH = 0%) and humid air (RH = 80%) on each sample are normalized using the peak around  $1390\text{ cm}^{-1}$  as a reference (Fig. 5d–f). The lower panel shows the difference spectra between these extreme RH values to illustrate the modifications induced by water exposure only. Note that the comparison between the samples based on difference spectra should be treated with caution since their respective references had different amounts of initially adsorbed water.

Upon water vapor exposure, an increase of O–H bending ( $1620\text{--}1650\text{ cm}^{-1}$ ) and stretching ( $3000\text{--}3600\text{ cm}^{-1}$ ) modes of water molecules is clearly observed. The O–H bending mode maximum in the difference spectra is observed at  $1624$ ,  $1630$  and  $1650\text{ cm}^{-1}$ , for CDs-COOH, CDs-NH<sub>2</sub> and CDs-OH, respectively. The O–H bending band of water molecules is known to shift toward higher frequency in the case of stronger hydrogen bonding.<sup>51</sup> Associated with the increase in O–H

bending is the generation of a water overtone feature in the region  $2000\text{--}2200\text{ cm}^{-1}$  for CDs-COOH and CDs-OH. For CDs-NH<sub>2</sub>, this water overtone band is located close to that of the amino group (around  $1900\text{ cm}^{-1}$ ), and thus leads to a band broadening.

The O–H stretching region is also sensitive to the hydrogen bonding environment of adsorbed water molecules.<sup>27,52</sup> It consists of three components peaking at  $3250$ ,  $3420$  and  $3540\text{ cm}^{-1}$ . The lowest component at  $3250\text{ cm}^{-1}$  is assigned to the water molecules having a HB coordination number similar to ice. The component at the highest frequency ( $3540\text{ cm}^{-1}$ ) is conversely ascribed to the HB environment in poorly connected water molecules such as in small water clusters. In between the two extreme frequencies lies a third component ( $3420\text{ cm}^{-1}$ ) which is associated with the HB interaction stronger than that of water clusters but weaker than that of network water.<sup>53–55</sup> For CDs-COOH and CDs-NH<sub>2</sub>, the weakly-bonded components ( $3420$  and  $3540\text{ cm}^{-1}$ ) are enhanced significantly after humid air exposure. For CDs-OH, the middle feature shows a red-shift of  $-36\text{ cm}^{-1}$  down to  $3380\text{ cm}^{-1}$ , together with a strong increase of the component at  $3250\text{ cm}^{-1}$ , indicating the appearance of strongly hydrogen bonded water molecules as compared to CDs-COOH and CDs-NH<sub>2</sub>. However, it should be noted that for the CDs-COOH sample, the different spectra were most probably related to intermolecular bonding between H<sub>2</sub>O molecules since the reference spectrum already contained a strong contribution from adsorbed water molecules.

In addition to the increase of water OH vibrational modes, surface-related modes are influenced by HB formation with water. After exposure to water, the C=O peak maximum of

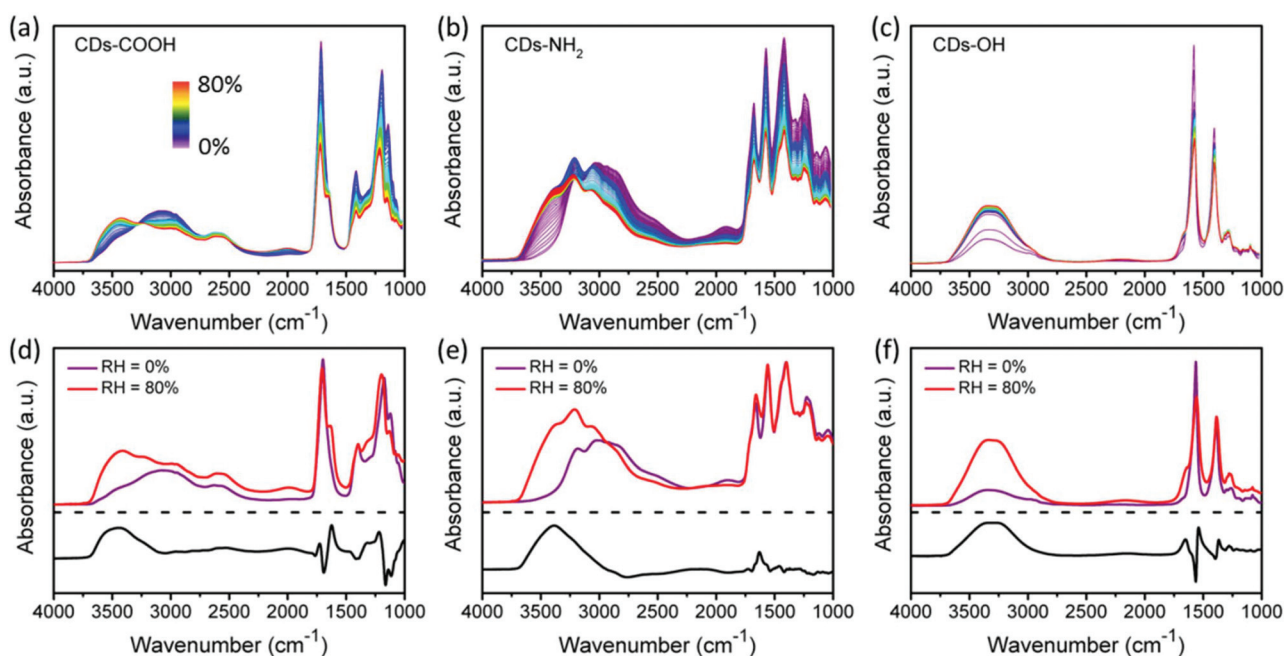


Fig. 5 (a)–(c) FTIR spectra of carbon dot samples recorded at different relative humidity values; (d)–(f) normalized FTIR spectrum obtained from the dry state and that from a humid atmosphere; the lower panel shows the difference spectrum.



CDs-COOH and CDs-OH is found to exhibit a shift of +8 and  $-6\text{ cm}^{-1}$ , respectively, while the band for CDs-NH<sub>2</sub> does not shift. In particular, C=O bonds are known to shift to lower frequency when accepting HBs,<sup>50</sup> which could be used to explain the red-shift of C=O stretching in CDs-OH. While they are related to carbonyl groups in CDs-OH, most C=O bonds in CDs-COOH are part of carboxyl groups connecting with OH groups, which supply more sites for HB formation upon water vapor exposure. While the hydroxyl oxygen and hydrogen can each form one a HB, it may change the angle and/or the length of the HBs with the C=O bond. These deformed HBs induce a higher frequency for C=O stretching than those of the corresponding HB interactions with a few water molecules (RH = 0%).<sup>50,56</sup> In addition, the C-O stretching band ( $1174\text{ cm}^{-1}$ ) of the carboxyl group in CDs-COOH is also enhanced with the exposure to water vapor due to hydrogen bonding, and shows a blue-shift of  $22\text{ cm}^{-1}$ .<sup>57</sup>

Based on the previous discussion, CDs-COOH forms the strongest HBs with water molecules, which cannot be fully removed from the CD surface even under dry air flow or vacuum at room temperature. After exposure to humid air, a stronger HB network is observed on CDs-OH; therefore the following ordering, from the strongest to weakest HB interactions with water, is proposed:



### pH-Dependence of the photoluminescence

In order to further clarify the correlation between the PL behavior and the surface groups of blue luminescent CDs, the influence of pH on the fluorescence spectra of three CDs was also investigated (Fig. 6). This reveals distinct differences among the three CD samples. While the PL of CDs-COOH is quenched at an increasing pH value, the PL of CDs-OH and CDs-NH<sub>2</sub> diminishes under both acidic and alkaline conditions. This pH effect correlates well with the protonation and deprotonation of the different functional groups. The carboxyl groups of CDs-COOH are deprotonated at pH 14, leading to a reduction in fluorescence. The PL intensity of CDs-NH<sub>2</sub> is stronger at the initial pH 8. Under both acidic and alkaline conditions, the PL is quenched uniformly throughout the whole emission range reflecting the amphoteric nature of amino groups.

Since the electrostatic attraction between negatively charged hydroxyl groups and positively charged protons under acidic conditions leads to the formation of non-radiative complexes, the peak II (427 nm) in CDs-OH was significantly reduced under acidic conditions in contrast to the alkaline conditions. It can be concluded that charged surface groups, either positively or negatively, tend to quench the luminescence compared to neutral groups. Note that the emission peak II at 420 nm also slightly shifts with varying pH, which could be related to different HB strengths with C=O groups.

### Understanding the photoluminescence behaviors of carbon dot samples

Comparing the X-ray and IR spectroscopic results with the fluorescence emission spectra helps interpret the differences in PL behaviors among the three CD samples. All CDs have three clear emission peaks shown in Fig. 1. CDs-COOH has the largest percentage of the conjugated system, identified from XAS. Consequently, the major emission component in CDs-COOH is peak III at 463 nm, assigned to the contribution from the conjugated carbon core. The  $n-\pi^*$  emission peak (II) centered at a lower wavelength (433 nm) is also strong for the CDs-COOH sample, which is mainly associated with carboxyl groups. These results confirm that the blue fluorescence of CDs-COOH mainly originates from the graphitic core and the C=O bonds, which is in good agreement with previous reports.<sup>24,46,58</sup> The surface-related emission (II) plays the predominant role in CDs-NH<sub>2</sub> (420 nm) and CDs-OH (427 nm) but appears shifted compared to CDs-COOH because C=O groups have a different bonding configuration. Note that the amino groups and hydroxyl groups grafted onto the carbogenic core can also enhance the integrity of the conjugated system as the electron donors, and thus induce a clear emission at 463 nm in CDs-NH<sub>2</sub> and CDs-OH as well.<sup>15,59</sup> Feature I at around 385 nm originates from an  $n-\sigma^*$  transition. This peak is more intense in CDs-NH<sub>2</sub> and CDs-OH which agrees with the XPS and XAS results. In the O K-edge XAS the  $\sigma^*$  intensity of CDs-OH is much stronger than those of the other two samples; C-O also dominates in O 1s XPS in CDs-OH. Similar results are observed in CDs-NH<sub>2</sub>.

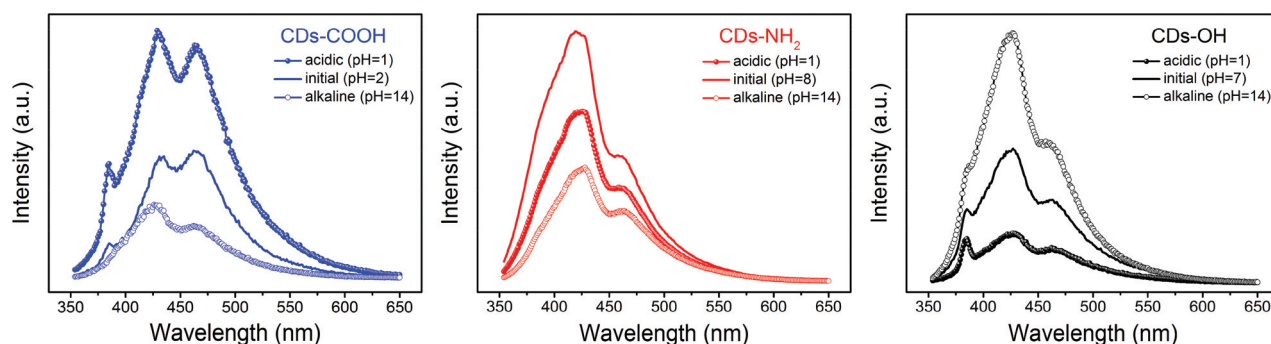


Fig. 6 pH-Dependent PL spectra of carbon dots under acidic (pH = 1) and alkaline (pH = 14) conditions; excitation was at 338 nm.



The spectral shift of PL emission II in the three CDs may be related to the C=O in different HB environments modified with the neighboring surface groups.<sup>25,54</sup> Sciortino *et al.* showed that excited states are sensitive to the solvent environment, leading to an emission shift.<sup>60</sup> Different local HB networks formed by surrounding water molecules with the surface groups may also influence the fluorescence behavior. A stronger HB is formed between CD samples and water, the PL is lower and a narrower emission energy level is generated, resulting in larger red shifts. Thus, the spectral shifts of peak II, whose emission maximum is located at 433 nm in CDs-COOH, 427 nm in CDs-OH and 420 nm in CDs-NH<sub>2</sub>, could be related to hydrogen bonding with water molecules as they follow the same order as the HB strength.

## Experimental

### Materials

The three aqueous dispersions (5 mg mL<sup>-1</sup>) of carbon dots with different surface chemistry (CDs-OH: GNQD0101, CDs-COOH: GNQD0301, and CDs-NH<sub>2</sub>: GNQD0201) were purchased from ACS Materials (USA), and used without further purification or treatment except when mentioned specifically. Note that in this paper, the samples were labelled CDs and not graphene quantum dots as stated by the provider because of the lack of evidence of a 2D structure. Ultrapure water purified using a PURELAB Plus system (ELGA) was used. The water resistivity was 0.300 ± 0.050 μS cm<sup>-1</sup>.

### Characterization techniques

The UV-vis absorption spectra were recorded on an OceanOptics USB 4000 UV-vis spectrometer. The fluorescence spectra were measured on an FLS920 fluorescence spectrometer (Edinburgh Instruments) with a MCP-PMT as a detector. A 450 W xenon lamp coupled to double monochromators was employed as the excitation light source. The slit widths at both excitation and emission were 4 nm. For pH dependent PL measurement, 10 M HCl and NaOH solution was used to adjust the pH value.

### Fourier transform infrared spectroscopy

Fourier transform infrared spectra were measured on a Bruker VERTEX 70v spectrometer using the attenuated total reflectance mode with a ZnSe crystal. For each sample, a reference spectrum was first acquired from a clean ZnSe crystal. A drop of CD dispersion (100 μL, 5 mg mL<sup>-1</sup>) was then drop-cast on the crystal and dried overnight. Spectra of dry samples were recorded under a flow of dry air (without CO<sub>2</sub>). The environmental ATR cell allows for the *in situ* detection of changes in the surface chemistry of the samples at different relative humidity values recorded at the outlet of the environmental cell. Humid air (RH over 80%) was generated by purging dry air through deionized water. After each sample, the ZnSe crystal was cleaned with ethanol, acetone, and water and a new reference spectrum was measured to validate the removal of all CD samples. The spectral resolution was set to 4 cm<sup>-1</sup>. 128

scans on dry CD samples and 32 scans for *in situ* measurements were collected.

### Synchrotron-based soft X-ray absorption and emission spectroscopy

X-ray absorption and emission spectroscopy measurements were performed on solid samples drop cast on conductive Si wafer. The data were collected at a U49/2 PGM1 beamline of a BESSY II synchrotron radiation source using a LiXEdrom end-station equipped with the Rowland circle geometry and area-sensitive multi-channel-plate photon detectors.<sup>62</sup> The beamline is connected to an undulator and equipped with a plane grating monochromator that offers soft X-rays from 85 to 1600 eV with a typical photon flux of 10<sup>13</sup> photons per s and a resolution ( $E/\Delta E$ ) better than  $2.5 \times 10^4$  below 500 eV. In this work, all XA spectra are obtained from total electron yield (TEY) mode. TEY-XAS was performed by scanning the samples in the energy ranges of 276–310 eV (for the C K-edge), 395–420 eV (for the N K-edge), and 528–552 eV (for the O K-edge) in 0.1 eV steps. The XA spectra in the figures have been normalized to the non-resonant part before and after the main features. Non-resonant XE spectra were measured within 5 minutes with excitation energy values of 310 eV (for the C K-edge), 420 eV (for the N K-edge) and 550 eV (for the O K-edge). Energies of XE spectra were calibrated using the elastic scattering peaks. XE spectra were normalized to unity for the maximum inelastic emission peak in each spectrum.

### X-ray photoemission spectroscopy

XPS results were measured in a CISSY setup<sup>63</sup> using Mg Kα radiation (1253.6 eV) as the excitation source and a CLAM 4 analyzer (VGScienta) with a 9-channeltron detector for the determination of electron kinetic energies, operated in an analysis chamber at a base pressure of 10<sup>-9</sup> mbar. The calibration of the energy scale was done using Au photoemission lines. The charging effect was corrected for all spectra. Photoemission lines of C, N and O 1s were recorded with a pass energy of 20 eV. Typical features in each spectrum were fit to a Gaussian–Lorentzian peak (30% Gaussian) after a Shirley-type background subtraction to extract the binding energy.

### Computational details

Theoretical calculations on carbon K-edge XAS were performed in 28 different model molecules of both coronene and circum-coronene sizes for a total of 1049 carbon atoms as discussed in more detail in ref. 28. The molecular structure was first optimized using density functional theory (DFT) with the Ahlrichs def2-SVP basis set and the TPSS meta-GGA functional. Then, the electronic structure was optimized in the more accurate def2-TZVP basis set with the BH<sup>0.57</sup>LYP functional.<sup>61</sup> The 1s core orbitals are then localized with the Pipek–Mezey localization scheme to ensure that excitation processes can be mapped locally to specific carbon atoms. Finally, in 1049 separate calculations, each of the 1s electrons is then locally excited into the fully available virtual orbital space using linear-response time-dependent DFT by calculating the first





150 transitions. This way, we obtain individual-atom XA spectra that can be directly correlated with the local functionalization pattern – and thus to the local electronic structure of the virtual orbital space. All calculations were performed using the ORCA suite 4.0.0.2.<sup>64</sup>

## Conclusions

In summary, this work demonstrates that the surface chemistry plays an essential role in the optical, chemical and electronic properties of CDs. A detailed study on the electronic structure of CDs is presented based on X-ray spectroscopy, and contributions from core and surface groups were described. The PL of three CDs was discussed based on the nature of the electronic states in the bandgap region. The HB interaction between CDs and water and pH-dependent PL spectra illustrate the surface-dependent properties of CDs. While all exhibit a blue luminescence, which could be related to the clear C=O signature in all CDs, the results presented herein demonstrate that surface chemistry could be used to finely tune the acceptor/donor electronic states and HB behavior of CDs. In addition to UV-Vis and IR spectroscopy, we expect that further studies using soft X-ray spectroscopy are needed for the rational design of CDs towards versatile applications. Future work will focus on the *in situ* X-ray spectroscopic study on CDs in aqueous solutions to probe the impact of solvation on the electronic structure of CDs.

## Conflicts of interest

There are no conflicts to declare.

## Acknowledgements

This project was funded by the Volkswagen Foundation (Freigeist Fellowship No. 89592 and No. 89525). Ute Resch-Genger and Florian Weigert acknowledges financial support by the M-era.Net project ICENAP (GA 1289/3-1, German Research Council, DFG). The authors thank HZB for the allocation of synchrotron radiation beamtime. Assistance provided by staff members of the BESSY II Synchrotron Facility is also gratefully acknowledged. We thank Dr E. Ritter and Dr U. Schade for the UV-vis absorption measurements and technical help with FTIR spectroscopy.

## References

- 1 S. N. Baker and G. A. Baker, *Angew. Chem., Int. Ed.*, 2010, **49**, 6726–6744.
- 2 H. Li, Z. Kang, Y. Liu and S.-T. Lee, *J. Mater. Chem.*, 2012, **22**, 24230–24253.
- 3 S. Zhu, Y. Song, X. Zhao, J. Shao, J. Zhang and B. Yang, *Nano Res.*, 2015, **8**, 355–381.
- 4 L. Xiao and H. Sun, *Nanoscale Horiz.*, 2018, **3**, 565–597.
- 5 K. Holá, Y. Zhang, Y. Wang, E. P. Giannelis, R. Zboril and A. L. Rogach, *Nano Today*, 2014, **9**, 590–603.
- 6 S. Zhu, Q. Meng, L. Wang, J. Zhang, Y. Song, H. Jin, K. Zhang, H. Sun, H. Wang and B. Yang, *Angew. Chem., Int. Ed.*, 2013, **52**, 3953–3957.
- 7 A. M. Chizhik, S. Stein, M. O. Dekaliuk, C. Battle, W. Li, A. Huss, M. Platen, I. A. T. Schaap, I. Gregor, A. P. Demchenko, C. F. Schmidt, J. Enderlein and A. I. Chizhik, *Nano Lett.*, 2016, **16**, 237–242.
- 8 W. F. Zhang, H. Zhu, S. F. Yu and H. Y. Yang, *Adv. Mater.*, 2012, **24**, 2263–2267.
- 9 X. Zhang, Y. Zhang, Y. Wang, S. Kalytchuk, S. V. Kershaw, Y. Wang, P. Wang, T. Zhang, Y. Zhao, H. Zhang, T. Cui, Y. Wang, J. Zhao, W. W. Yu and A. L. Rogach, *ACS Nano*, 2013, **7**, 11234–11241.
- 10 S. Ghosh, A. M. Chizhik, N. Karedla, M. O. Dekaliuk, I. Gregor, H. Schuhmann, M. Seibt, K. Bodensiek, I. A. T. Schaap, O. Schulz, A. P. Demchenko, J. Enderlein and A. I. Chizhik, *Nano Lett.*, 2014, **14**, 5656–5661.
- 11 H. Yu, R. Shi, Y. Zhao, G. I. N. Waterhouse, L.-Z. Wu, C.-H. Tung and T. Zhang, *Adv. Mater.*, 2016, **28**, 9454–9477.
- 12 J. Liu, Y. Liu, N. Liu, Y. Han, X. Zhang, H. Huang, Y. Lifshitz, S.-T. Lee, J. Zhong and Z. Kang, *Science*, 2015, **347**, 970–974.
- 13 G. A. M. Hutton, B. Reuillard, B. C. M. Martindale, C. A. Caputo, C. W. J. Lockwood, J. N. Butt and E. Reisner, *J. Am. Chem. Soc.*, 2016, **138**, 16722–16730.
- 14 K. A. Ritter and J. W. Lyding, *Nat. Mater.*, 2009, **8**, 235–242.
- 15 S. Zhu, J. Zhang, S. Tang, C. Qiao, L. Wang, H. Wang, X. Liu, B. Li, Y. Li, W. Yu, X. Wang, H. Sun and B. Yang, *Adv. Funct. Mater.*, 2012, **22**, 4732–4740.
- 16 Y. Wang, S. Kalytchuk, Y. Zhang, H. Shi, S. V. Kershaw and A. L. Rogach, *J. Phys. Chem. Lett.*, 2014, **5**, 1412–1420.
- 17 S. K. Cushing, M. Li, F. Huang and N. Wu, *ACS Nano*, 2014, **8**, 1002–1013.
- 18 D. Qu, M. Zheng, J. Li, Z. Xie and Z. Sun, *Light: Sci. Appl.*, 2015, **4**, e364.
- 19 S. Qu, D. Zhou, D. Li, W. Ji, P. Jing, D. Han, L. Liu, H. Zeng and D. Shen, *Adv. Mater.*, 2016, **28**, 3516–3521.
- 20 V. Strauss, J. T. Margraf, C. Dolle, B. Butz, T. J. Nacken, J. Walter, W. Bauer, W. Peukert, E. Spiecker, T. Clark and D. M. Guldi, *J. Am. Chem. Soc.*, 2014, **136**, 17308–17316.
- 21 D. Pan, J. Zhang, Z. Li and M. Wu, *Adv. Mater.*, 2010, **22**, 734–738.
- 22 S. Wang, I. S. Cole, D. Zhao and Q. Li, *Nanoscale*, 2016, **8**, 7449–7458.
- 23 J. Zhong, H. Zhang, X. Sun and S.-T. Lee, *Adv. Mater.*, 2014, **26**, 7786–7806.
- 24 H. Ding, S.-B. Yu, J.-S. Wei and H.-M. Xiong, *ACS Nano*, 2016, **10**, 484–491.
- 25 T. Zhang, J. Zhu, Y. Zhai, H. Wang, X. Bai, B. Dong, H. Wang and H. Song, *Nanoscale*, 2017, **9**, 13042–13051.
- 26 F. Zaera, *Chem. Rev.*, 2012, **112**, 2920–2986.
- 27 T. Petit, L. Puskar, T. A. Dolenko, S. Choudhury, E. Ritter, S. Burikov, K. Laptinskiy, Q. Brzustowski, U. Schade,





- H. Yuzawa, M. Nagasaka, N. Kosugi, M. Kurzyp, A. Venerosy, H. A. Girard, J.-C. Arnault, E. Osawa, N. Nunn, O. Shenderova and E. F. Aziz, *J. Phys. Chem. C*, 2017, **121**, 5185–5194.
- 28 F. Weber, J. Ren, T. Petit and A. Bande, submitted.
- 29 C.-H. Chuang, Y.-F. Wang, Y.-C. Shao, Y.-C. Yeh, D.-Y. Wang, C.-W. Chen, J. W. Chiou, S. C. Ray, W. F. Pong, L. Zhang, J. F. Zhu and J. H. Guo, *Sci. Rep.*, 2014, **4**, 4525.
- 30 V. Lee, L. Whittaker, C. Jaye, K. M. Baroudi, D. A. Fischer and S. Banerjee, *Chem. Mater.*, 2009, **21**, 3905–3916.
- 31 H.-K. Jeong, H.-J. Noh, J.-Y. Kim, M. H. Jin, C. Y. Park and Y. H. Lee, *Europhysics Lett.*, 2008, **82**, 67004.
- 32 C.-H. Chuang, S. C. Ray, D. Mazumder, S. Sharma, A. Ganguly, P. Papakonstantinou, J.-W. Chiou, H.-M. Tsai, H.-W. Shiu, C.-H. Chen, H.-J. Lin, J. Guo and W.-F. Pong, *Sci. Rep.*, 2017, **7**, 42235.
- 33 R. P. Gandhiraman, D. Nordlund, C. Javier, J. E. Koehne, B. Chen and M. Meyyappan, *J. Phys. Chem. C*, 2014, **118**, 18706–18712.
- 34 D. Pacilé, M. Papagno, A. F. Rodríguez, M. Grioni, L. Papagno, Ç. Ö. Girit, J. C. Meyer, G. E. Begtrup and A. Zettl, *Phys. Rev. Lett.*, 2008, **101**, 66806.
- 35 D. A. Outka, J. Stöhr, R. J. Madix, H. H. Rotermund, B. Hermsmeier and J. Solomon, *Surf. Sci.*, 1987, **185**, 53–74.
- 36 A. Ganguly, S. Sharma, P. Papakonstantinou and J. Hamilton, *J. Phys. Chem. C*, 2011, **115**, 17009–17019.
- 37 D. Pacilé, J. C. Meyer, A. Fraile Rodríguez, M. Papagno, C. Gómez-Navarro, R. S. Sundaram, M. Burghard, K. Kern, C. Carbone and U. Kaiser, *Carbon*, 2011, **49**, 966–972.
- 38 J. MacNaughton, A. Moewes and E. Z. Kurmaev, *J. Phys. Chem. B*, 2005, **109**, 7749–7757.
- 39 X. Liang, Y. Wang, H. Zheng and Z. Wu, *J. Electron Spectrosc. Relat. Phenom.*, 2014, **196**, 89–93.
- 40 H. Liu, T. Ye and C. Mao, *Angew. Chem., Int. Ed.*, 2007, **46**, 6473–6475.
- 41 E. J. McDermott, E. Z. Kurmaev, T. D. Boyko, L. D. Finkelstein, R. J. Green, K. Maeda, K. Domen and A. Moewes, *J. Phys. Chem. C*, 2012, **116**, 7694–7700.
- 42 L. Zhang, N. Schwertfager, T. Cheiwchanchamnangij, X. Lin, P.-A. Glans-Suzuki, L. F. J. Piper, S. Limpijumnong, Y. Luo, J. F. Zhu, W. R. L. Lambrecht and J.-H. Guo, *Phys. Rev. B: Condens. Matter Mater. Phys.*, 2012, **86**, 245430.
- 43 W. T. Hong, K. A. Stoerzinger, B. Moritz, T. P. Devereaux, W. Yang and Y. Shao-Horn, *J. Phys. Chem. C*, 2015, **119**, 2063–2072.
- 44 K. Holá, M. Sudolská, S. Kalytchuk, D. Nachtigallová, A. L. Rogach, M. Otyepka and R. Zbořil, *ACS Nano*, 2017, **11**, 12402–12410.
- 45 D. Usachov, O. Vilkov, A. Grüneis, D. Haberer, A. Fedorov, V. K. Adamchuk, A. B. Preobrajenski, P. Dudin, A. Barinov, M. Oehzelt, C. Laubschat and D. V. Vyalikh, *Nano Lett.*, 2011, **11**, 5401–5407.
- 46 H. Ding and H.-M. Xiong, *RSC Adv.*, 2015, **5**, 66528–66533.
- 47 J.-J. Max and C. Chapados, *J. Phys. Chem. A*, 2004, **108**, 3324–3337.
- 48 F. Wang, Z. Xie, H. Zhang, C. Liu and Y. Zhang, *Adv. Funct. Mater.*, 2011, **21**, 1027–1031.
- 49 B. C. M. Martindale, G. A. M. Hutton, C. A. Caputo and E. Reisner, *J. Am. Chem. Soc.*, 2015, **137**, 6018–6025.
- 50 B. Nie, J. Stutzman and A. Xie, *Biophys. J.*, 2005, **88**, 2833–2847.
- 51 M. Laporta, M. Pegoraro and L. Zanderighi, *Phys. Chem. Chem. Phys.*, 1999, **1**, 4619–4628.
- 52 D. B. Asay and S. H. Kim, *J. Phys. Chem. B*, 2005, **109**, 16760–16763.
- 53 J.-B. Brubach, A. Mermet, A. Filabozzi, A. Gerschel and P. Roy, *J. Chem. Phys.*, 2005, **122**, 184509.
- 54 D. B. Asay, A. L. Barnette and S. H. Kim, *J. Phys. Chem. C*, 2009, **113**, 2128–2133.
- 55 A. Anderson and W. R. Ashurst, *Langmuir*, 2009, **25**, 11549–11554.
- 56 P. Hobza and Z. Havlas, *Chem. Rev.*, 2000, **100**, 4253–4264.
- 57 L. George and W. Sander, *Spectrochim. Acta, Part A*, 2004, **60**, 3225–3232.
- 58 X. Miao, D. Qu, D. Yang, B. Nie, Y. Zhao, H. Fan and Z. Sun, *Adv. Mater.*, 2017, **30**, 1704740.
- 59 Q.-L. Zhao, Z.-L. Zhang, B.-H. Huang, J. Peng, M. Zhang and D.-W. Pang, *Chem. Commun.*, 2008, 5116–5118.
- 60 A. Sciortino, E. Marino, B. van Dam, P. Schall, M. Cannas and F. Messina, *J. Phys. Chem. Lett.*, 2016, **7**, 3419–3423.
- 61 N. A. Besley and F. A. Asmuruf, *Phys. Chem. Chem. Phys.*, 2010, **12**, 12024–12039.
- 62 E. F. Aziz, J. Xiao, R. Golnak and M. Tesch, Helmholtz-Zentrum Berlin für Materialien und Energie, *J. Large-Scale Res. Facil.*, 2016, **2**, A80.
- 63 I. Lauermaun and A. Steigert, Helmholtz-Zentrum Berlin für Materialien und Energie, *J. Large-Scale Res. Facil.*, 2016, **2**, A67.
- 64 F. Neese, *Mol. Sci.*, 2018, **8**, e1327, DOI: 10.1002/wcms.1327.

